

AFRL-ML-WP-TP-2007-471

**INITIAL EXAMINATION OF THE
STRENGTH OF SINGLE-ENDED
SOURCES IN MICROMETER-SIZED
SINGLE CRYSTALS (Preprint)**



**S.I. Rao, D.M. Dimiduk, M. Tang, T.A. Parthasarathy, M.D. Uchic,
and C. Woodward**

APRIL 2007

Approved for public release; distribution is unlimited.

STINFO COPY

The U.S. Government is joint author of this work and has the right to use, modify, reproduce, release, perform, display, or disclose the work.

**MATERIALS AND MANUFACTURING DIRECTORATE
AIR FORCE RESEARCH LABORATORY
AIR FORCE MATERIEL COMMAND
WRIGHT-PATTERSON AIR FORCE BASE, OH 45433-7750**

REPORT DOCUMENTATION PAGE					<i>Form Approved</i> OMB No. 0704-0188				
The public reporting burden for this collection of information is estimated to average 1 hour per response, including the time for reviewing instructions, searching existing data sources, gathering and maintaining the data needed, and completing and reviewing the collection of information. Send comments regarding this burden estimate or any other aspect of this collection of information, including suggestions for reducing this burden, to Department of Defense, Washington Headquarters Services, Directorate for Information Operations and Reports (0704-0188), 1215 Jefferson Davis Highway, Suite 1204, Arlington, VA 22202-4302. Respondents should be aware that notwithstanding any other provision of law, no person shall be subject to any penalty for failing to comply with a collection of information if it does not display a currently valid OMB control number. PLEASE DO NOT RETURN YOUR FORM TO THE ABOVE ADDRESS.									
1. REPORT DATE (DD-MM-YY) April 2007		2. REPORT TYPE Journal article preprint		3. DATES COVERED (From - To)					
4. TITLE AND SUBTITLE INITIAL EXAMINATION OF THE STRENGTH OF SINGLE-ENDED SOURCES IN MICROMETER-SIZED SINGLE CRYSTALS (Preprint)				5a. CONTRACT NUMBER FA8650-04-D-5233					
				5b. GRANT NUMBER					
				5c. PROGRAM ELEMENT NUMBER 62102F					
6. AUTHOR(S) S.I. Rao and T.A. Parthasarathy (UES, Inc.) D.M. Dimiduk and M.D. Uchic (Metals Development Section (AFRL/MLLMD)) M. Tang (Lawrence Livermore National Laboratory) C. Woodward (Northwestern University)				5d. PROJECT NUMBER 2311					
				5e. TASK NUMBER 00					
				5f. WORK UNIT NUMBER 23110002					
7. PERFORMING ORGANIZATION NAME(S) AND ADDRESS(ES) <div style="display: flex; justify-content: space-between;"> <div style="width: 45%;"> UES, Inc. 4401 Dayton-Xenia Road Dayton, OH 45432-1894 </div> <div style="width: 45%;"> Metals Development Section (AFRL/MLLMD) Lawrence Livermore National Laboratory Northwestern University </div> </div>				8. PERFORMING ORGANIZATION REPORT NUMBER					
9. SPONSORING/MONITORING AGENCY NAME(S) AND ADDRESS(ES) Materials and Manufacturing Directorate Air Force Research Laboratory Air Force Materiel Command Wright-Patterson AFB, OH 45433-7750				10. SPONSORING/MONITORING AGENCY ACRONYM(S) AFRL-ML-WP					
				11. SPONSORING/MONITORING AGENCY REPORT NUMBER(S) AFRL-ML-WP-TP-2007-471					
12. DISTRIBUTION/AVAILABILITY STATEMENT Approved for public release; distribution is unlimited.									
13. SUPPLEMENTARY NOTES PAO Case Number: AFRL/WS 07-1142, 07 May 2007. Paper contains color. The U.S. Government is joint author of this work and has the right to use, modify, reproduce, release, perform, display, or disclose the work.									
14. ABSTRACT A recent study indicated that the behavior of single-ended dislocation sources contributes to the flow strength of micrometer-scale crystals. In this study 3D discrete dislocation dynamics simulations are used to calculate the effects of anisotropy of dislocation line tension on the strength of single-ended dislocation sources in micrometer-sized volumes with free surfaces, and to compare them with the strength of double-ended sources of equal length. This is done by directly modeling their plastic response within a 1-micron cubed volume composed of a single crystal FCC metal. In general, double-ended sources are stronger than single-ended sources of an equal length and exhibit no significant effects from truncating the long-range elastic fields at this scale. The double-ended source strength increases with Poisson ratio, exhibiting an increase of about 50% at $\nu = 0.38$ (value for Ni) as compared to the value at $\nu = 0$. Independent of dislocation line direction, for ν greater than 0.20, the strengths of single-ended sources depend upon the sense of the stress applied.									
15. SUBJECT TERMS Micrometer-sized crystals; 3D dislocation dynamics simulations; Single and double-ended sources; Anisotropic line energy; Image stresses									
16. SECURITY CLASSIFICATION OF: <table style="width: 100%; border-collapse: collapse;"> <tr> <td style="width: 33%; border: 1px solid black; padding: 2px;">a. REPORT Unclassified</td> <td style="width: 33%; border: 1px solid black; padding: 2px;">b. ABSTRACT Unclassified</td> <td style="width: 33%; border: 1px solid black; padding: 2px;">c. THIS PAGE Unclassified</td> </tr> </table>			a. REPORT Unclassified	b. ABSTRACT Unclassified	c. THIS PAGE Unclassified	17. LIMITATION OF ABSTRACT: SAR	18. NUMBER OF PAGES 40	19a. NAME OF RESPONSIBLE PERSON (Monitor) John Barnes 19b. TELEPHONE NUMBER (Include Area Code) (937) 255-9791	
a. REPORT Unclassified	b. ABSTRACT Unclassified	c. THIS PAGE Unclassified							

ESTIMATING THE STRENGTH OF SINGLE-ENDED DISLOCATION SOURCES IN MICROMETER-SIZED SINGLE CRYSTALS

S.I. Rao*, D.M. Dimiduk, M. Tang#, T.A. Parthasarathy*,
M.D. Uchic and C. Woodward^

Air Force Research Laboratory, Materials and Manufacturing Directorate,
AFRL/MLLM Wright-Patterson AFB, OH 45433-7817

*UES, Inc., 4401 Dayton-Xenia Rd, Dayton, OH 45432-1894

#Lawrence Livermore National Laboratory, P.O. Box 808, L-45 Livermore, CA 94551

^Northwestern University, Department of Materials Science and Engineering, 2220
Campus Drive, Evanston, IL 60208-3108

Abstract

A recent study indicated that the behavior of single-ended dislocation sources contributes to the flow strength of micrometer-scale crystals. In this study 3D discrete dislocation dynamics simulations are used to calculate the effects of anisotropy of dislocation line tension (increasing Poisson's ratio, ν) on the strength of single-ended dislocation sources in micrometer-sized volumes with free surfaces, and to compare them with the strength of double-ended sources of equal length. This is done by directly modeling their plastic response within a 1 micron³ volume composed of a single crystal FCC metal. In general, double-ended sources are stronger than single-ended sources of an equal length and exhibit no significant effects from truncating the long-range elastic fields at this scale. The double-ended source strength increases with Poisson ratio (ν), exhibiting an increase of about 50% at $\nu = 0.38$ (value for Ni) as compared to the value at $\nu = 0$. Independent of dislocation line direction, for ν greater than 0.20, the strengths of single-ended sources depend upon the sense of the stress applied. The value for α , in the

PREPRINT

expression for strength, $\tau = \alpha(L)\mu b/L$ is shown to vary from 0.4 to 0.84 depending upon the character of the dislocation and the direction of operation of the source at $\nu = 0.38$ and $L = 933b$. By varying the lengths of the sources from 933 to $233b$, it was shown that the scaling of the strength of single-ended and double-ended sources with their length both follow a $\ln(L/b)/(L/b)$ dependence. Surface image stresses are shown to have little effect on the critical stress of single-ended sources at a length of $\sim 250b$ or greater. This suggests that for 3D discrete dislocation dynamics simulations of the plastic deformation of micrometer sized crystals in the size range, $0.5 - 20\mu\text{m}$, image stresses making the surface traction-free can be neglected. The relationship between these findings and a recent statistical model for the hardening of small volumes is also discussed.

Keywords: Micrometer-sized crystals; 3D dislocation dynamics simulations; Single and double-ended sources; Anisotropic line energy; Image stresses

1.0 Introduction

Recent experimental studies discovered that the proximity of free surfaces bounding small volumes at the micrometer scale produces strong size-affected strengthening in face-center cubic (FCC) single crystals, even for high initial dislocation densities [1-8]. In an unpublished study [9], the present authors used large scale 3D dislocation dynamics simulations (DDS) to explicitly model the deformation behavior of micrometer-sized crystals. In that work two underlying mechanisms that give rise to free-surface size effects were identified. One mechanism—surface-mediated source hardening—was found to be especially potent in micrometer-scale volumes. This effect arises from the conversion of pre-existing double-ended dislocation sources into single-ended sources that intersect and interact with free surfaces. Such a conversion establishes a new

characteristic length for the dislocation sources. The sources were shown to adopt configurations that are related to those previously described for small constrained volumes by Blankenhagen, et. al., [10] but with a key difference being that the dislocation lines are truncated by intersecting the free surfaces. In samples below a critical size, the truncation of dislocation sources, together with the under-sampling of an assumed initially random distribution of dislocation sources, leads to smaller average source lengths when compared to a bulk sample of equal dislocation density. This surface-mediated source-hardening contribution was analytically modeled and shown to account for a significant portion of the strengthening observed in FCC micrometer sized crystals [11]. However, for those calculations, the dislocation line tensions were taken to be isotropic and the strength of single-ended dislocation sources of a length ' L ' was assumed to be $\alpha\mu b/L$, where α is of the order of 1, μ is the shear modulus and ' L ' is the length of the single-ended source [11]. Further, those findings were based upon 3D DDS results that used a simplifying assumption of neglecting image forces for the behavior of the dislocations that intersected the surfaces of the simulation cell. This assumption was necessary for efficient parallel computation of large simulation cells that better represented deforming microcrystals by having free surfaces rather than periodic boundary conditions. In order to lay the foundation for critical analysis of large scale 3D-DDS simulations of freestanding micro-columns, this paper explores the actual source strengths that may be expected for small volumes that contain principally single-armed sources that intersect a surface. Previously, the strengths of single-ended and double-ended sources were modeled using isotropic elastic theory, at a value of Poisson's ratio of 0.333 [12]. These strengths have been evaluated for the special case of a glide plane

intersecting the surface at right angles in a semi-infinite-half-space material. As a result, a simple image construction was possible for that analysis to include the influence of image forces on source strength. The study shows that the strengths of single-ended sources are dependent upon the direction of traverse of the source and are weaker than those of double-ended sources by a factor of 1.3 - 2.6 [12]. That study also showed that the scaling of the strength of both single-ended and double-ended sources with their length follows a $\ln(L/b)/(L/b)$ dependence. However, within a current broader context, it is desirable to isolate the influence of the image stress from the overall behavior of the dislocation sources and to understand the behavior of such sources for more general dislocation configurations. This is motivated by the significant computational overhead required to accurately account for image forces in a large scale 3D-DDS calculation. It is highly desirable to employ simpler approximations that are easily implemented in a parallel architecture, while maintaining a reasonable level of accuracy.

Accordingly, in this work a DDS technique is used to calculate the effects of anisotropy of dislocation line tension (within the isotropic elasticity assumption) on the strengths of single-ended sources and, to compare them with the strengths of double-ended sources of equal length. This is done by directly modeling their plastic response within a 1 x 1 x 1 micron volume of FCC Ni single crystal with {001} surfaces where the glide plane intersects the surface at a crystallographically-appropriate angle of 54.7°. A comparison of simulation results with an accurate consideration of image stresses, here called Full Free Surface Treatment (FFST), with similar results that did not include consideration of image stresses, here called Simplified Surface Approximation (SSA) is performed. The FFST and SSA results are in turn compared with the previous findings

on strengths of single-ended sources by Pichaud et. al., [12] and the implications of these results are discussed.

2.0 Simulation technique

A version of the 3-dimensional parallel DDS code “ParaDiS,” [13,14] developed at Lawrence Livermore National Laboratory, was used to simulate the stress-strain response of single-ended and double-ended sources in a cubic crystal volume with edge lengths equal to 1 micron. In ParaDiS, dislocation lines are represented as a series of nodal points connected by straight-line segments. The glide-plane force on each node is calculated using isotropic linear elasticity and the velocity of a node is taken to be linearly proportional to the force according to a viscous damping law. In these simulations, the velocity was set at $4000\ b/s$ for a force due to an applied shear stress of 1 Pa, where b is the magnitude of the Burgers vector of the gliding dislocation (0.25 nm). For these simulations the shear modulus and Poisson’s ratio were set to values of 59.9 GPa and 0.38, respectively. These values correspond to the shear modulus $= \mu_{111}$ for Ni and Poisson’s ratio, $\nu = c_{12}/(c_{11}+c_{12})$, where c_{11} and c_{12} are the cubic single-crystal elastic constants of Ni [15]. To describe anisotropic elasticity effects correctly in the isotropic approximation for double-ended sources, Scattergood and Bacon [16] suggest using an isotropic shear modulus as $\mu = 4\pi E_{screw}/b^2$ and, Poisson’s ratio, ν , as $1 - E_{screw}/E_{edge}$, where E_{screw} and E_{edge} are the pre-logarithmic line energy factors for infinite straight $a/2\langle 110 \rangle$ screw and edge dislocations on the $\{111\}$ plane in FCC Ni. Such calculations give $\mu = 78.7$ GPa and $\nu = 0.38$ for Ni. Therefore, critical stresses given in this manuscript for single-ended and double-ended sources at a Poisson’s ratio of 0.38,

must be scaled to a shear modulus of 78.7 GPa from a shear modulus of 59.9 GPa, to obtain their absolute values in Ni.

For these simulations, a constant strain rate of 50 s^{-1} was imposed along the [41-3] crystal direction. The (1-1-1)[110] slip system is maximally stressed under these conditions, having a Schmidt factor of 0.47. Both the single-ended and double-ended sources in the simulation were operative on this slip system. If at any time step, the specimen plastic displacement rate was lower than the applied rate, the applied stress was incremented to obey a constant applied displacement rate. However, if the specimen plastic displacement rate was higher than that of the programmed rate, the applied stress was kept constant, thus permitting source expansion. Increments in stress occurred only after it was determined that the total displacement at a particular time was less than the applied displacement rate multiplied by the elapsed time.

The ParaDiS code was modified in the following manner to qualitatively account for dislocation surface effects (the SSA). This approximation to the dislocation-surface interaction is useful because including the details of image effects in large-scale parallel DDS of dislocation ensembles evolving over significant strains is computationally challenging. This is particularly true for the range of simulation cell sizes required to describe the size scaling effects observed in recent micro-compression experiments in FCC metals; where these microcrystals range in size from 0.2 – 20 μm diameter [1-8]. As dislocation segments expand they eventually reach the surface, and those that lay on the surface are deleted as though they exited the glide plane of the dislocation source. Further, within the SSA method, the velocity of the terminal dislocation node at the surfaces (surface nodes) is modified such that the velocity components perpendicular to

both the free surface and the glide plane were zero, causing the node to track the surface trace of the slip plane. As described in Section 4 we found that the SSA treatment, not only qualitatively captures the most important free surface effect of establishing a new critical source length for flow, but is also computationally efficient within a parallel environment. Separate simulations using a serial version of ParaDiS were used to show that small changes in the strength of single armed sources can be expected due to the influence of the image forces acting on dislocations from free surfaces (our FFST method). Selected source configurations acting under the influence of image forces were examined to quantify these effects. The image stresses were modeled using a hybrid technique where the singular and non-singular parts of the image stresses are dealt with separately [17]. The analytic solution for a semi-infinite straight dislocation intersecting the surface of elastic half-space is used to account for the singular part of the image stress, while the remaining non-singular part is treated using the standard finite-element method [17]. As described in Section 4, the effect of the image force acting on a single-arm source was found to decrease the source strength by less than $\sim 10\%$ when compared with the SSA method. Comparison of the dislocation configuration at the critical point shows that the dislocation is slightly longer in the case where image stresses are included.

3.0 Sources within the simplified surface approximation

One objective for this work was to determine the effect of the line energy anisotropy on the strength of single-ended and double-ended dislocation sources in small material volumes. Consequently, four types of simulations were conducted; i) double-ended sources for both isotropic and anisotropic line energies, ii) single-ended sources for both

isotropic and anisotropic line energies, iii) single-ended sources of varying line orientation with anisotropic line energy and finally, iv) single-ended and double-ended sources of varying line length with anisotropic line energy. For the first case analytical results exist in the literature for an equivalent configuration acting within an infinite volume and these are used for comparison. The infinite-volume case has also been extended to include an expression for the effect of Poisson's ratio on the double-ended source strength based on prior simulation studies. In the isotropic limit, the strength of a single-armed source is expected to be half that of a double-ended source of the same length. These prior results were verified for a small volume and then the effects of dislocation line energy anisotropy and line character on both double-ended and single-ended sources are examined. Three dislocation characters, edge, screw and 30° mixed dislocation characters were considered.

3.1 Double-ended sources in a small volume

The source strengths for double-ended sources in small crystals were calculated using sources of length $933b$, approximately one-fourth the cube edge length, placed at the center of a cube of material, whose sides were 1 micron in length. Note that for this source geometry, the double-ended source achieved its critical configuration without intersecting the free-surface. The effect of Poisson's ratio was calculated using a 30° mixed-character dislocation and the results are shown in Fig. 1. For the double-ended sources in an infinite medium, the critical stress as a function of Poisson's ratio can be written as [16]

$$\tau(\nu) = \frac{\alpha\mu b}{L} = \frac{\mu b}{L} C \left(\frac{3}{4(1-\nu)} + \frac{1}{4} \right) \quad (1)$$

A fit of equation 1 to the simulated critical stress data for double-ended sources is shown in Fig. 1 and the correspondence is very good for a value of $C = 0.823$. Thus, the influence of the finite volume is negligible for double-ended sources that are completely contained within the boundaries of the crystal at the 1 micrometer scale and above.

3.2 Single-ended sources in a small volume

Critical stresses were evaluated for the single-ended sources as a function of Poisson's ratio, keeping the source length constant at $933b$. The results are shown in Fig. 2, for the case of a source whose initial configuration was a straight line extending from a fixed node inside the cube to the surface and the line character being a 30° mixed dislocation. The strength of this source depended upon both the sign of the applied stress that resulted in the 'forward' or 'reverse' operation of the source, and the degree of line anisotropy. The results are shown in comparison to a double-ended source, which has the same critical stress for both forward and reverse operation. As shown by Fig. 2, one may observe that for the case of isotropic line tension ($\nu = 0.1$), the source strength of a single-armed dislocation source is nearly half that of the equivalent length double-ended source. This result is in agreement with published estimates of the critical stress for single-ended sources in a line energy isotropic material [18]. Further there is no significant difference between the forward and reverse directions for the isotropic line tension case.

However, for the anisotropic line energy case ($\nu > 0$), Fig. 2 shows that for the forward direction, the critical stresses increase rapidly with increasing Poisson's ratio (similar to those for double-ended sources). However, for the reverse direction, the source strengths increase more gradually. When ν is large (> 0.3), the critical stresses for single-ended sources are more than half of those for double-ended sources when stresses act in the forward direction and, less than half when stresses act in the reverse direction, when the Poisson's ratio is large (> 0.3). These results are similar to the simulation results of Pichaud et. al., [12] who considered the case of a Poisson's ratio of 0.333. Note that for all of the FCC microcrystals used in experimental studies reported in the literature, viz., Cu, Ni, Au and Al [1-8], ν is relatively large (> 0.3) and the anisotropy in critical stress between the forward and reverse directions for the 30° degree single-ended source is expected to occur. This result suggests that there is an intrinsic scatter to the source strengths even for fixed source lengths.

3.3 Origin of source strength asymmetry

For the small volumes examined here, the stress-strain curves and dislocation configurations at the critical stress offer insights into the nature of the source-strength asymmetry with respect to the direction of operation. Consider a single-ended source of length $933b$, inserted into a one micron cubic simulation cell ($\nu = 0.38$), residing on a $\{111\}$ plane and having its fixed point inside the cell and the other end on the $\{100\}$ surface. For the 30° mixed-character dislocation line source, this source has a line direction $\langle 211 \rangle$ which is 30° away from the $\langle 110 \rangle$ screw-line direction and perpendicular to the surface edge trace, a $\langle 01-1 \rangle$ direction. Figure 3 shows the stress-

strain response of the forward and reverse operation of such a source along with a pure screw character single-ended source. The stress-versus-strain response of the forward operating 30° source was purely elastic-plastic with a critical stress of 114 MPa (CRSS of 54.5 MPa in Fig. 2). At the critical stress, the single ended-source completely traverses the (1-1-1) glide plane leading to uncontrolled plastic deformation of the microcrystal volume. The stress-strain response of the screw-character source was qualitatively similar to the forward operating source save for a critical stress of 90 MPa (CRSS of 42.3 MPa in Fig. 2). In this case, the Burgers vector of the initial source was chosen, for convenience, to be a $\langle 211 \rangle$ direction such that the initial source had a screw-character direction. For the 30° reverse source, the sign of the input Burgers vector was reversed as compared to 30° forward source, such that the source moves in the opposite direction under the same applied stress. Unlike the other two single-ended sources, the stress-strain curve shows a small strain burst at 57 MPa (CRSS of 27.2 MPa in Fig. 2) before uninhibited plastic deformation at 64 MPa (CRSS of 30.6 MPa in Fig. 2).

Figure 4 shows the initial (stress free) and critical configuration (maximum stress) of these sources. The results show that at the very beginning of the simulation, when the applied stress is almost zero, both 30° sources rotate from their initial line direction to the screw-character position, a $\langle 110 \rangle$ direction. This occurs because of the lower line-energy per-unit-length for the screw-character dislocation. It is known in the literature that the most frequently observed surface effect for dislocations is Lothe's force which causes dislocations to rotate to lower their line energy [19]. Thus, the energy increase due to the necessary line length increase as it rotates is more than offset by the energy decrease due to line direction change, from 30° to zero degrees. For the screw-character

source case, no rotation needs to occur since the initial line direction is the low-energy configuration. The critical configurations for these sources are shown in Fig. 4. Note that the line tension forces tend to curve the sources about the fixed point and the screw-character direction. Upon application of the applied stress, the direction of traverse for the single-ended source acting in the 30° forward case is such that the source initially decreases its line length. However, for the 30° reverse source, the source is moving in a direction that continually increases line length as it travels toward the critical configuration. Therefore, the asymmetry in the critical stress between the 30° forward and reverse directions of motion is most probably related to line tension forces. These forces make it easier for the source to curve in a direction with increasing line length as compared to a direction with decreasing line length. For the screw-character case, the source is curving about the fixed point and the initial direction, which has a line length intermediate to the previous two cases and, the corresponding critical stress of 90 MPa lies between 114 MPa (30° forward) and 57 MPa (30° reverse). For both the 30° forward and screw-character cases, once the source overcomes the critical configuration, it continuously traverses the glide plane leading to uninhibited plastic deformation. For the 30° reverse case, once the source overcomes the critical configuration shown in Fig. 4, it traverses the glide plane and reaches another critical configuration on the opposite surface edge, which corresponds to (in our nomenclature) a 30° forward source for the opposite surface edge, with a larger length. The second critical position is overcome at a stress of 64 MPa and thereafter, the source continuously traverses the glide plane.

These results suggest that for $\nu = 0.38$ (i.e. pure Ni), the 30° single-ended source has strengths of approximately $0.8\mu b/L$ in the forward direction and $0.4\mu b/L$ in the reverse direction, while double-ended sources are stronger than the corresponding single-ended sources.

4.0 Effect of image stresses using the full free surface treatment

In the previous section, calculations of the plastic response of single-ended sources of length $933b$ in a 1 micron cubic cell were presented. For those simulations the image stresses that make the surface traction-free were not considered. For the set of simulations presented in this section, the images forces were included by the following method. A different serial version of the ParaDiS code with a hybrid technique [17] for calculating the image stresses was employed. The hybrid technique considers the image-stress field as a superposition of analytic and FEM based solutions. The analytic solution is the image-stress field of a semi-infinite straight dislocation intersecting the free surface of a semi-infinite half-space. The geometry of this dislocation is chosen such that its image stress contains the same singularity as the image stress of the dislocation of interest. The second, FEM solution, is the difference between these two image stress fields and by construction it is a non-singular function of space and converges much faster than a direct FEM calculation of the complete image-stress field [17, 20].

When image stresses are also considered for the simulation cell, there are minor differences in the exact configurations and critical stresses adopted by dislocation sources. For example, the 30° single-ended source does not rotate all the way to the screw-character line position as was seen in the earlier SSA-method calculations. Rather,

that source rotates to a position $10\text{-}15^\circ$ away from the screw-character position (see Fig. 5). With image forces imposed, the source tries to lie orthogonal to the cell surface [12], but these forces are resisted by line tension forces that push the line toward the screw-character position. Thus, the balancing of these two forces results in an initial position which is in between the initial 30° position and the screw-character position and thereby a slightly altered source length. Under continued increase in stress, the source then bows around this initial configuration and the fixed point to attain the critical configuration at a stress of 104 MPa (CRSS of 49.7 MPa in Fig. 2). The final distance to the surface at the critical configuration is slightly larger as compared to the SSA-method case, resulting in a slight decrease of the critical stress ($\sim 10\%$). For the 30° reverse case, the critical stress with the FFST is slightly larger, 60 MPa (CRSS of 28.7 MPa in Fig. 2), as compared to the results from the SSA method. In this case, the stress increases as a result of both the image and line energy forces tended to work against the applied stress, thus reducing the source length relative to the image-free source. Figure 6 shows the critical stresses using the FFST method for the 30° forward and 30° reverse cases, which are similar to the results shown in Fig.2. A direct comparison of the source critical stresses between these two figures reveals that within the present image-force analysis there is only a modest effect when image stresses are included. Overall, image stresses have only a slight effect ($< \sim 10\%$) on the critical stresses of single-ended sources at these sizes.

Prior studies of image-force effects reported in the literature [19] suggest that image stresses decrease rapidly as one moves away from the free surface, taking on a value of only about 10 MPa for distance of about $50 - 100b$ away from the free surface. This

distance is equivalent to 1 or 2 nodes at or near the surface for the discretization lengths typically used in the present (and other) DDS simulations. Since the source length considered here is an order of magnitude larger than this image-stress decay distance, it is not surprising that image stresses have little effect on the critical stress of single-ended sources of length $933b$. They are expected to become more significant as the source length is decreased below $\sim 250b$. In spite of these results showing a negligible influence of the image stresses, it is important to note an alternate effect that was not investigated in the present study. From prior studies, image stresses are also known to significantly increase the propensity for screw-character dislocations to cross-slip near surfaces. This occurs by the image forces acting to constrict the Shockley partials of the $a/2\langle 110 \rangle$ screw-character dislocation at some surfaces [19, 21, 22]. Dislocation cross-slip has not been considered in the simulation results presented here. Any cross-slip at or near the surface due to image stresses may result in a complete or partial pinning of the dislocation at the point of surface intersection, thus raising the strengths of single-ended sources toward those of a double-ended source of the same length. Thus, the present results from both the SSA and FFST methods must be viewed only as plausible lower bounds on single-ended source strengths.

5.0 Length scaling of the critical stress of single-ended and double-ended sources

Figure 7 shows a plot of the critical resolved shear stress of double-ended (30°) and single-ended (30° forward and 30° backward) sources, as a function of source length

varying from 233 to $933b$, at $\nu = 0.38$. Also shown in the plot are fits to the simulation data using an equation of the form

$$\tau(L) = k\mu \frac{\ln(L/b)}{(L/b)} \quad (2)$$

where k is a constant. It is seen that equation (3) fits the simulation data very well, with k being 0.06 for single-ended sources (backward), 0.12 for single-ended sources (forward) and 0.18 for double-ended sources. From prior literature reports, it is well known that the critical stresses of double-ended sources scale according to equation (2) [23, 24]. Figure 7 shows that scaling according to equation (2) is also valid for single-ended sources as was observed in the simulations of Pichaud, et. al., [12] for lengths varying between $10^3 - 10^6b$. Also note that the simulations leading to Fig. 7 were performed using the SSA method. As discussed before, image stresses are expected to influence the strength of single-ended sources only when the lengths of the sources reach $\sim 250b$ or less. Therefore, equation (2) can be considered valid for single-ended sources, for source lengths greater than $500b$, as used for analysis of the Ni microcrystals [11].

6.0 Source strength coefficients for single-ended and double-ended sources at a Poisson's ratio of 0.38

For dislocation sources, the balance between dislocation line length and line curvature leads to the following expression for the critical resolved shear stress versus source length:

$$\tau(L) = \frac{\alpha\mu b}{L} \quad (3)$$

where ‘ L ’ is the length of the single-ended or double-ended source. The parameter ‘ α ’ is the source-strength coefficient that varies with the exact nature of the source, length of the source and the material. For these simulations, the value of Poisson’s ratio was fixed at 0.38 and the values for α were determined at a length of $933b$. Table 1 shows values for the coefficient for various sources that indicate a variation from 0.4 – 0.84 for single-ended sources and, 0.8 – 1.28 for double-ended sources in small volumes. Clearly, the double-ended sources are stronger than the single-ended sources of the same length. The coefficient ‘ α ’ at any length of the single-ended or double-ended sources can be obtained from their corresponding value at $933b$ as

$$\alpha(L) = \alpha_{933b} \frac{\ln(L/b)}{6.84} \quad (4)$$

7.0 Discussion and summary

To open the discussion this study is summarized as follows:

1. The strengths of single- and double-ended dislocation sources were determined for a 1 micron cubic simulation cell using a 3D DDS code and a simplified treatment of surface conditions that is amenable to efficient parallel computing. The initial length of the sources was fixed at $933b$ for this cell and both the line energy anisotropy (Poisson’s ratio) and line character were varied.
2. Single-ended sources are weaker than the corresponding full Frank-Read sources, with the measure of strength ‘ α ’ for single ended sources varying between 0.4 – 0.84 and, for double ended sources varying between 0.86 – 1.28,

at a Poisson's ratio of 0.38. There was no observable influence from truncating an infinite volume at the 1 micrometer scale.

3. There is an asymmetry in the strength of single-ended sources depending upon the direction of traverse of the source. The direction where the source length initially decreases is stronger for Poisson's-ratio values greater than 0.2. This is in agreement with previous results from Pichaud et. al., [12] on the strength of single-ended sources for the special case of a glide plane intersecting the surface at right angles and a Poisson's ratio of 0.333.
4. For a separate set of simulations the near-surface image force was introduced and its influence on source strength was examined for a source length of $933b$ to check the effect of the SSA. At these source lengths, image stresses have a small effect ($<10\%$) on the strength of single-ended sources.
5. In the absence of image stresses, the scaling of the strength of single-ended and double-ended sources with their length follows a $\ln(L/b)/(L/b)$ dependence. This is in agreement with previous results from Pichaud et. al., [12] for source lengths ranging from $10^3 - 10^6b$.
6. Comparison of the present results on the strength of single-ended sources with previous results from Pichaud, et. al., [12] suggests that the strength of single-ended sources follows equation (2) with k given by (within 15%) [12]

$$k = 0.108 + 0.040\cos(2\phi + \pi/3) \quad (5)$$

where ' ϕ ' is the angle between the Burger's vector and line direction of the single-ended source, for source lengths greater than $500b$.

The single-ended sources envisaged here for micrometer-sized crystals are conceptually similar to the ones proposed by Blanckenhagen, et. al., [10] for the strengthening of constrained micrometer-scale volumes. Both concepts involve the setting of a new dislocation source length that is different from the initial source and governed by the presence of a constraining surface. However, there are significant quantitative differences between the constraints imposed by a grain boundary wherein the full dislocation loop is envisaged to be retained (such as in the work by Blankenhagen, et. al.), and those imposed at a free surface where the loop shape is lost and the dislocation may be free to move under a more gentle curvature. In the Blanckenhagen, et. al., model the impenetrable grain boundary sets a new smaller length for the operation of the Frank-Read source, for initial Frank-Read source sizes that are larger than $1/3$ the grain diameter. Thus, strengthening of the system occurs as the result of a constrained smaller source length. Herein, single-ended sources form with the dislocation being mobile on the free surface and thus are weaker than the corresponding Frank-Read sources of an equal length in the bulk. However, other simulations suggest that microcrystals that form such configurations are strengthened nonetheless [9].

These findings re-enforce the statistical model suggested by Parthasarathy et. al., [11] which used source-strength coefficients that are generally of the order of those calculated in this work. Thus, it is readily expected that the single-ended sources can result in hardening a small deforming volume provided that the stochastic aspects of that model are representative of physical microcrystals. In that model it is argued that sources form from an initial dislocation forest of some density and, even though single-ended sources are weaker than the corresponding Frank-Read sources of an identical length, the lengths

of single-ended sources found in microcrystals are, on average, much smaller than Frank-Read sources for a given dislocation density. This is illustrated by Fig. 8 (adapted from [11]) wherein the average length of single-ended sources, scaled by the diameter of the simulation cell, is plotted against the number of initial mobile sources in the sample, again for a fixed starting dislocation density. Also shown in Fig. 8 is the standard deviation in the source lengths as a function of number of initial mobile sources in the sample. Figure 8 clearly shows that as the number of initial mobile sources decreases, the average source length scaled to the diameter decreases significantly. As the number of initial mobile sources decreases (decreasing sample size), the strengths of single-ended sources becomes important, even though they are weaker than equivalent-length double-ended sources. Also as discussed previously, cross-slip induced by image stresses may increase the strengths of single-ended sources to levels that approach those of double-ended sources, thereby making the strength of single-ended sources even more important. Such effects remain to be investigated. Thus, for small micrometer-scale volumes, single-ended sources are expected to control plastic deformation and to lead to high initial stresses in micrometer-sized volumes [11].

In the statistical model of Parthasarathy et. al., [11] the strength of single-ended sources was taken to be approximately equal to $\langle \alpha \rangle \mu b / L$, where $\langle \alpha \rangle$ was taken to be 1. The range of sample diameters considered in the model was 1 – 20 microns and the sample radius was chosen as the maximum source length, L . From that statistical analysis, the average length of single-ended sources, over that range of sample diameters, is a factor of 5 – 10 larger than the value of $933b$ selected in this study. The simulations presented here give ' α ' in the range of 0.54 to 1.12 at a length of $9330b$ for single-ended

sources and the SSA (equation 4), with an average value of 0.83. Therefore, the value of 1 chosen for $\langle \alpha \rangle$ in [11] is a slight overestimate of the contribution of source-truncation hardening to the strengthening observed at small sizes in microcrystal experiments [1-8]. However, 3D dislocation dynamics studies [9] show that in addition to source-truncation hardening another mechanism of strengthening is present in micrometer sized crystals, ‘exhaustion hardening’, which is related to the cessation of initially-operating single-ended sources due to interaction with obstacles and the re-activation of these original sources or activation of new new sources at larger stresses. This second mechanism of strengthening has not been taken into account in the statistical model [11] and could account for discrepancy between the experimental strengthening data and the statistical model of Parthasarathy et. al.

ACKNOWLEDGEMENT

The authors acknowledge use of the 3D DDS code, ParaDiS, which was developed at Lawrence Livermore National Laboratory by the ParaDiS team. The work of M. Tang is performed under the auspices of the United States Department of Energy by the University of California. This work was supported by the AFOSR, and by a grant of computer time from the DOD High Performance Computing Modernization Program, at the Aeronautical Systems Center/Major Shared Resource Center. The work was performed at the U.S. Air Force Research Laboratory, Materials and Manufacturing Directorate, Wright-Patterson AFB.

REFERENCES

1. M. D. Uchic, D. M. Dimiduk, J. N. Florando and W. D. Nix, in: George, E. P., Inui, H., Mills, M.J. & Eggeler, G. editors. *Defect Properties and Related Phenomena in Intermetallic Alloys*, Materials Research Society Symposium Proceedings, vol. 753. Pittsburgh (PA): Materials Research Society p. 27 (2003).
2. M. D. Uchic and D. M. Dimiduk, Mater. Sci. Engr. A., **400–401** 268 (2005).
3. D. M. Dimiduk, M. D. Uchic and T.A. Parthasarathy, Acta Mater., **53** 4065 (2005).
4. D.M. Dimiduk, C. Woodward, R. LeSar and M.D. Uchic, Science, **312** 1188 (2006).
5. M.D. Uchic, D. M. Dimiduk, J.N. Florando and W.D. Nix, Science, **305** 986 (2004).
6. J.R. Greer, W.C. Oliver and W.D. Nix, Acta Mater., **53** 1821 (2005). Errata
7. C.A. Volkert and E. Lilliodden, Phil. Mag. **86**, 5567-5579 (2006).
8. D.M. Dimiduk, M.D. Uchic, S.I. Rao, C.Woodward and T.A. Parthasarathy, Modelling Simul. Mater. Sci. Eng., **15**, 135-146 (2007).
9. S.I. Rao, T.A. Parthasarathy, M. Tang, D.M. Dimiduk, M.D. Uchic and C. Woodward, to be submitted for publication (2007).
10. B.V. Blankenhagen, P. Gumbsch and E. Arzt, Phil.Mag.Letters, **83**, 1 (2003).
11. T.A. Parthasarathy, S.I. Rao, D.M. Dimiduk, M.D. Uchic and D.R. Trinkle, Scripta. Mater., **56**, 313 (2007).
12. B. Pichaud, F. Minari and J. Kellerhals, Phil.Mag.A, **38**, 593 (1978).
13. W. Cai, V. Bulatov, T. Pierce, M. Hiratani, M. Rhee, M. Bartelt and M. Tang, Massively-parallel dislocation dynamics simulations in Solid Mechanics and Its applications, edited by Kitagawa, H. & Shibutani, Y. (Kluwer Academic Publishers) **115**, 1 (2004).
14. A. Arsenlis, W. Cai, M. Tang, M. Rhee, T. Oppelstrup, G. Hommes, T.G. Pierce, and V.V. Bulatov, Modelling Simul. Mater.Sci.Eng., accepted for publication (2007).
15. A.J. Ardell, Metall.Trans. A, **16**, 2131 (1985).
16. D. Bacon, D. Barnett and R. Scattergood, Prog. Mater. Sci., **23**, 208 (1978).

17. M. Tang, W. Cai, G. Xu and V. Bulatov, *Modelling Simul. Mater. Sci. Eng.*, **14**, 1139 (2006).
18. J.P. Hirth and J. Lothe, *Theory of dislocations*, second edition, John Wiley and Sons, New York (1982).
19. P.M. Hazzledine, in *Fundamentals of Deformation and Fracture*, edited by B.A. Bilby, et al., C.U.P. 385 (1985).
20. M. Tang, G. Xu, W. Cai and V. Bulatov, in *Thin film stresses and mechanical properties* edited by Corcoran S G, Joo Y-C, Moody N R & Zuo Z (Materials Research Society, Warrendale, PA) **U2.4**, 795 (2003).
21. P.M. Hazzledine and S.J. Shaibani, in 6th International Conference on Strength of Metals and Alloys (ICSMA), ed. R.C. Gifkins (Oxford: Pergamon), **1**, 45 (1982).
22. P.M. Hazzledine, H.P. Karnthaler and E. Wintner, *Philos. Mag.*, **32**, 81-97 (1975).
23. E. Nembach, *Prog.Mater.Sci.*, **45**, 275 (2000).
24. R. Madec, B. Devincre and L.P. Kubin, *Phys. Rev. Let.*, **89**, 255508-1 (2002).

Figure captions

Figure 1: The critical resolved shear stress, $\tau^*(\nu)$ for a double-ended source having 30° mixed dislocation character as a function of Poisson's ratio. Critical stresses are in MPa. The line gives the best fit of the simulation-based empirical relation given by Bacon, et. al., (15) for infinite crystals, with $C = 0.823$. Results from FFST method are denoted by open symbols.

Figure 2: The critical resolved shear stress, $\tau^*(\nu)$ for single-ended source of 30° mixed character is shown compared with the result for double-ended source of the same length. Critical stresses are in MPa. Unlike the double-ended source, the single-ended source has

a different critical stress depending upon the forward or backward direction of operation. Results from FFST method are denoted by open symbols.

Figure 3: Stress-strain curves for three single-ended sources of length 933b, 30° forward, 30° reverse and screw character in a 1 micron cubic cell using the SSA method. Stresses are in MPa. Shear modulus = 59.9 GPa and Poisson's ratio = 0.38. The cubic cell was stressed in the [41-3] direction.

Figure 4: Critical configurations of a 30° single-ended source moving in the forward and reverse directions and a screw-character source of length 933b in a 1 micron cubic cell. Shear modulus is 59.9 GPa and Poisson's ratio = 0.38. The initial rotation of the 30° source is also depicted. All results are for the SSA method.

Figure 5: Comparison of the critical configurations of a 30° single-ended source moving in the forward direction with and without image stresses (both SSA & FFST methods). Shear modulus is 59.9 GPa and Poisson's ratio = 0.38. The initial rotation of the source is also depicted.

Figure 6: The critical resolved shear stresses, $\tau^*(\nu)$ for single-ended and double-ended (Frank-Read) sources of 30° mixed character and length 933b. Results shown are for $\nu = 0.1$ and 0.38. Image stresses are included in the simulations using the FFST method. Critical stresses are in MPa.

Figure 7: Critical resolved shear stress (τ^*) of 30° single-ended and double-ended (Frank-Read) sources as a function of length L of the sources. Also, shown are $k\mu\ln(L/b)/(L/b)$ fits to the simulation data (solid lines). $k = 0.06$ (single ended backward); $k = 0.12$ (single ended forward) and $k = 0.18$ (double ended). All results are for the SSA method. Critical stresses are in MPa.

Figure 8: a) Average source length, $\langle L \rangle$ (scaled to the radius of the sample, R) versus the number of initial mobile sources in the sample (based on an initial dislocation density [11]). b) Schematic illustration of source length probability distributions for microcrystals versus bulk samples following model given in [11].

Source	α (using SSA)
<i>Single-ended (30° forward)</i>	0.84
<i>Single-ended (30° reverse)</i>	0.4
<i>Single-ended (screw)</i>	0.66
<i>Frank-Read (screw)</i>	1.28
<i>Frank-Read (30°)</i>	1.19
<i>Frank-Read (edge)</i>	0.86

Table 1: Measure of strength of single-ended and Frank-Read sources, ' α ', at a Poisson's ratio, ν of 0.38 and length of 933b.

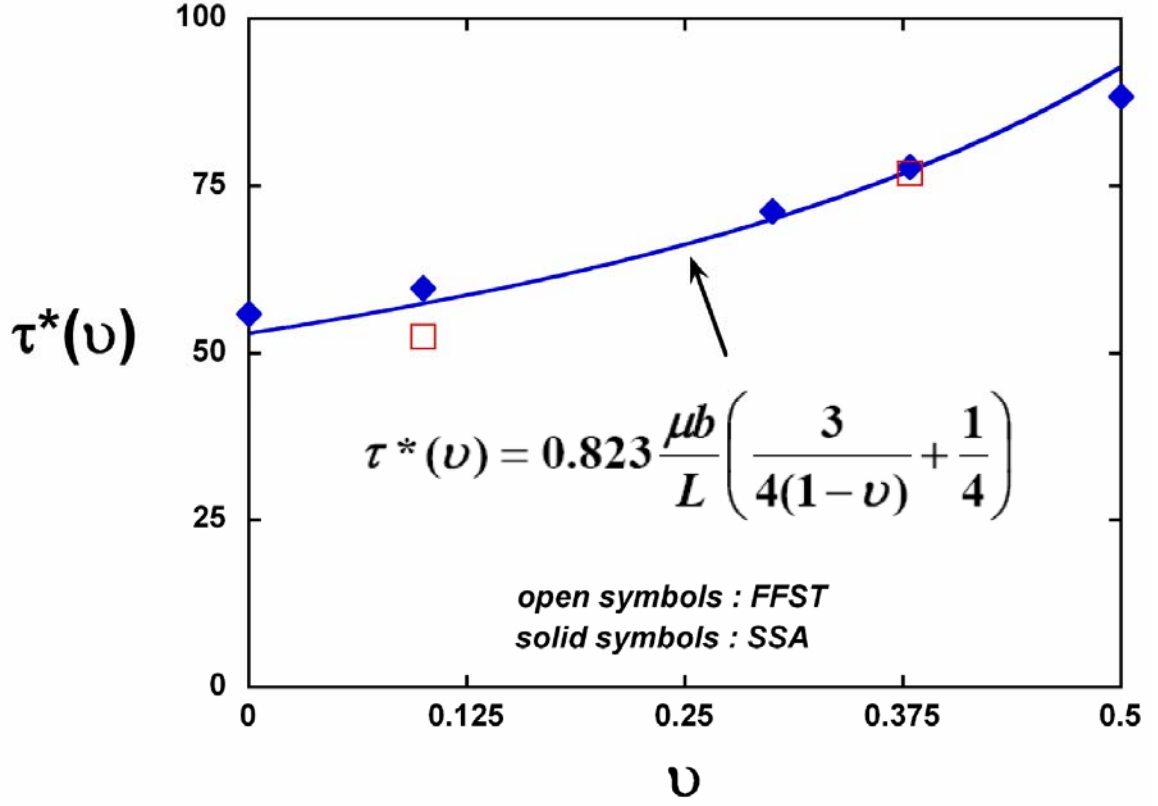


Figure 1: The critical resolved shear stress, $\tau^*(\nu)$ for a double-ended source having 30° mixed dislocation character as a function of Poisson's ratio using both the SSA and FFST. Critical stresses are in MPa. The line gives the best fit of the simulation-based empirical relation given by Bacon, et. al., (15) for infinite crystals, with $C = 0.823$.

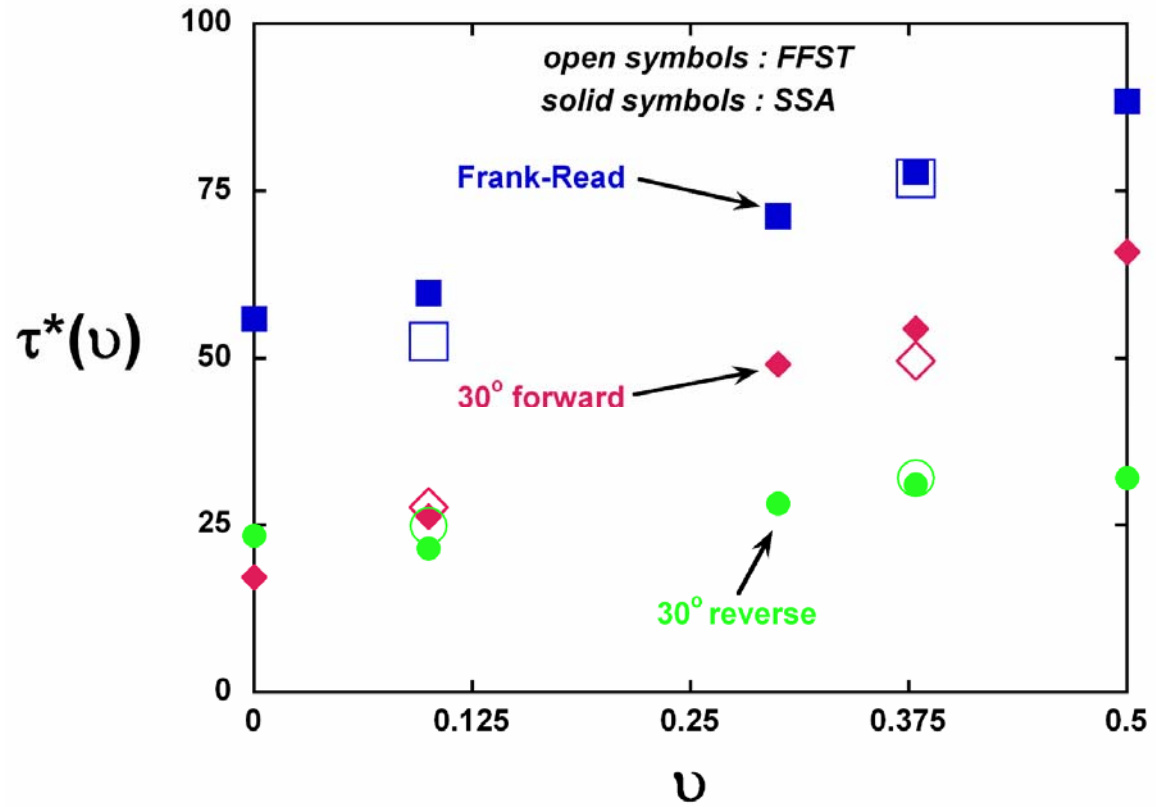


Figure 2: The critical resolved shear stress, $\tau^*(\nu)$ for single-ended source of 30° mixed character is shown compared with the result for double-ended source of the same length for both the SSA and FFST. Critical stresses are in MPa. Unlike the double-ended source, the single-ended source has a different critical stress depending upon the forward or backward direction of operation.

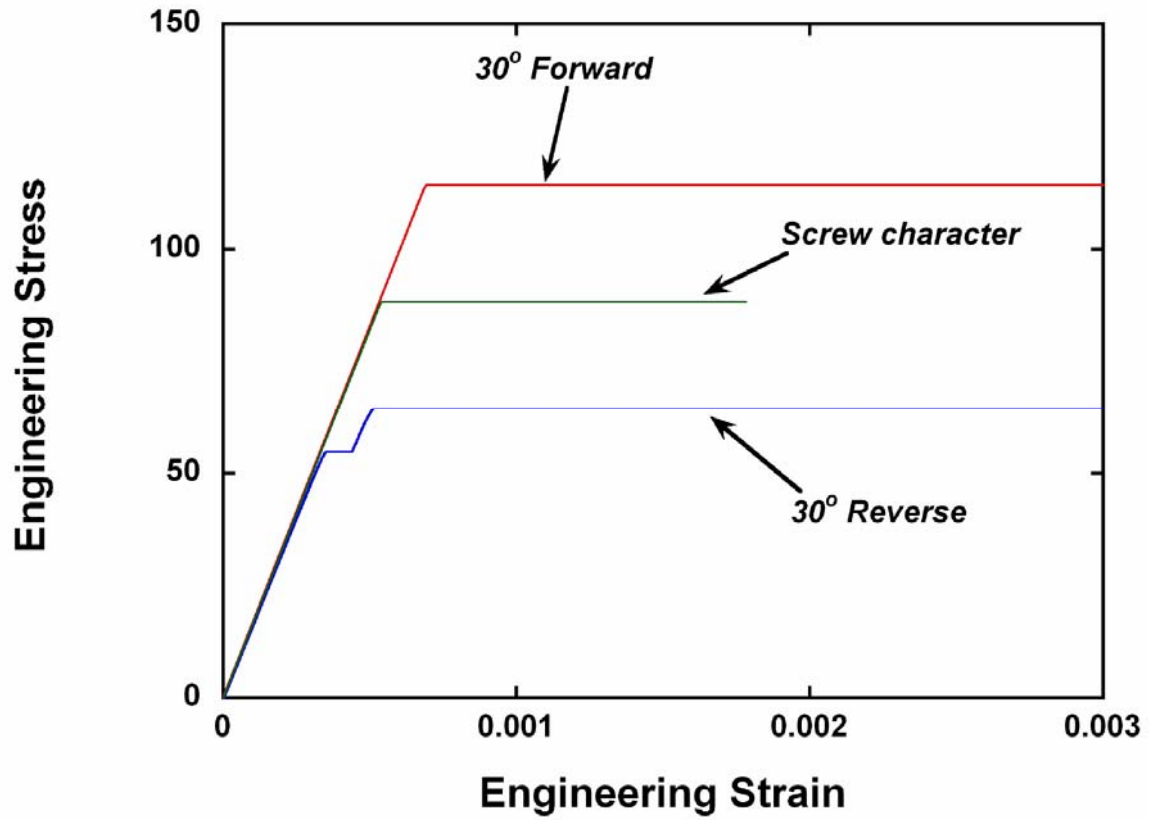


Figure 3: Stress-strain curves for three single-ended sources of length 933b, 30° forward, 30° reverse and screw character in a 1 micron cubic cell using the SSA method. Stresses are in MPa. Shear modulus = 59.9 GPa and $\nu = 0.38$. The cubic cell was stressed in the [41-3] direction.

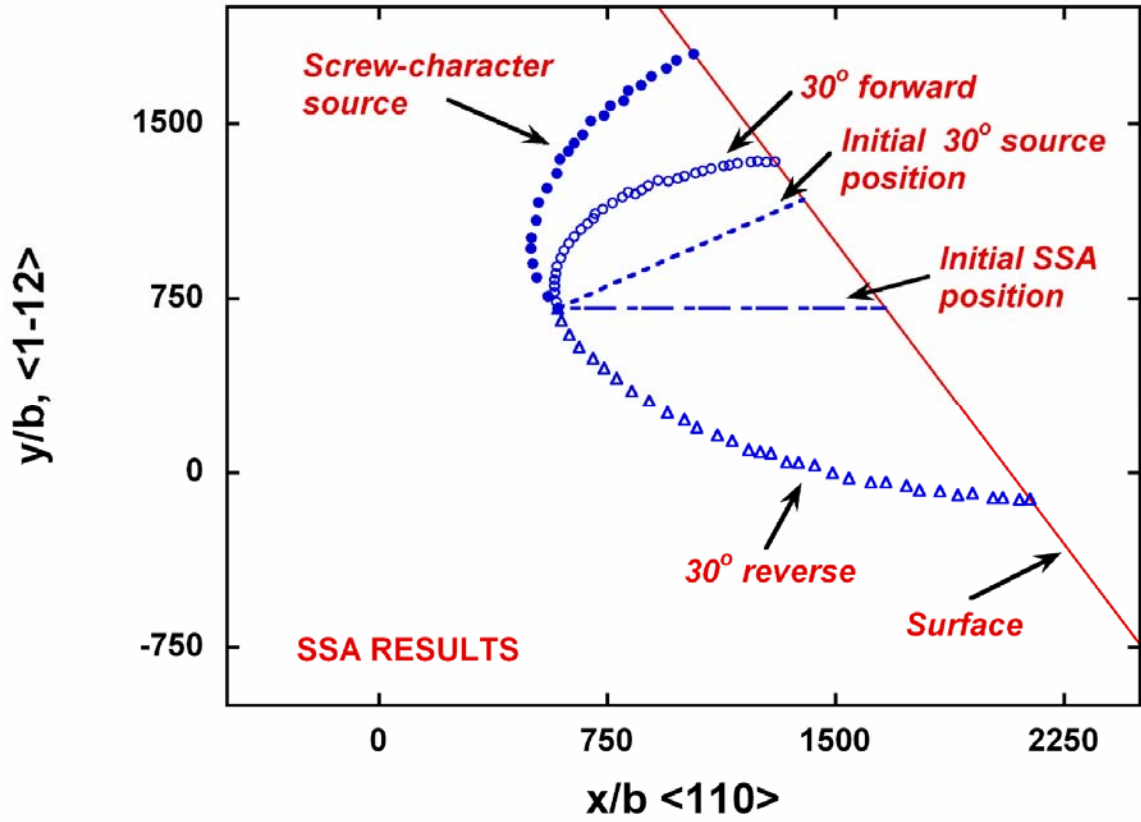


Figure 4: Critical configurations (curved lines) of a 30° single-ended source moving in the forward and reverse directions and a screw-character source of length $933b$ in a 1 micron cubic cell. Shear modulus is 59.9 GPa and $\nu = 0.38$. The initial rotation of the 30° source is also depicted. All results are for the SSA method.

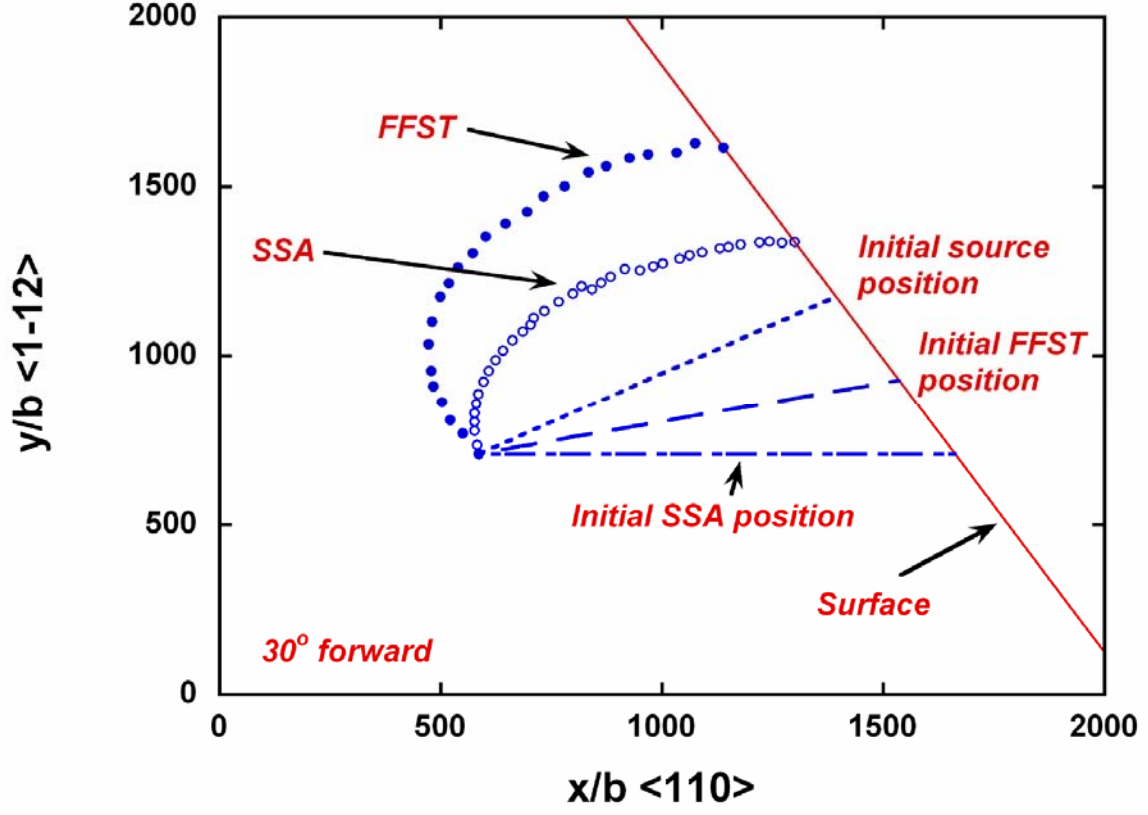


Figure 5: Comparison of the critical configurations (curved lines) of a 30° single-ended source moving in the forward direction with and without image stresses (both SSA & FFST methods). Shear modulus is 59.9 GPa and $\nu = 0.38$. The initial rotation of the source is also depicted, as discussed in text.

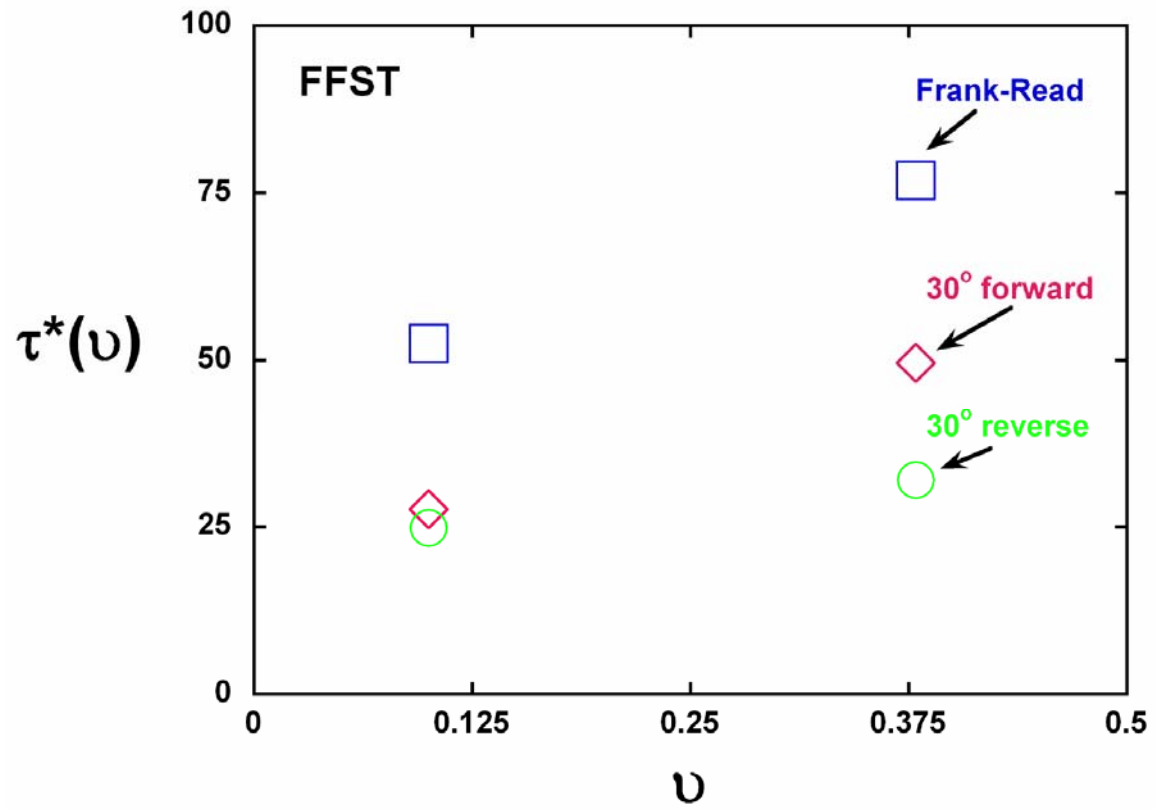


Figure 6: The critical resolved shear stresses, $\tau^*(\nu)$ for single-ended and double-ended (Frank-Read) sources of 30° mixed character and length 933b using the FFST method, where image stresses are included. Results shown are for $\nu = 0.1$ and 0.38 and critical stresses are in MPa.

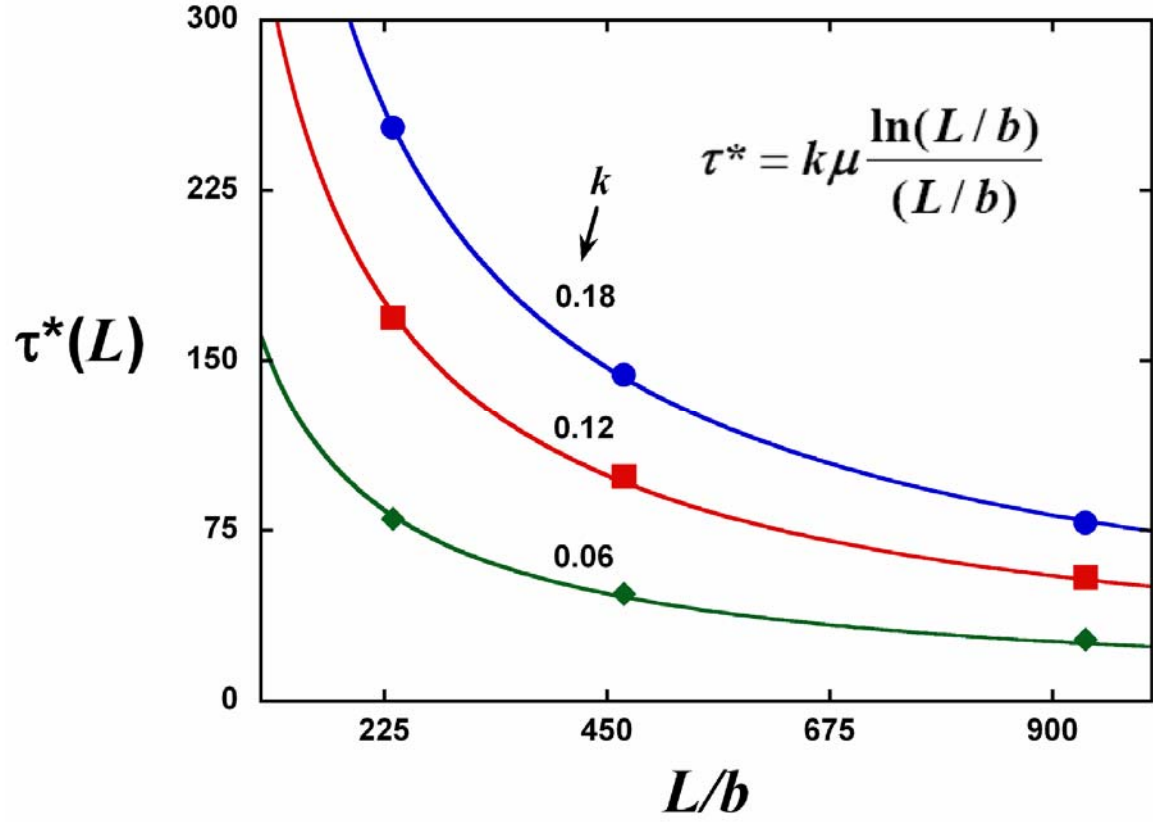
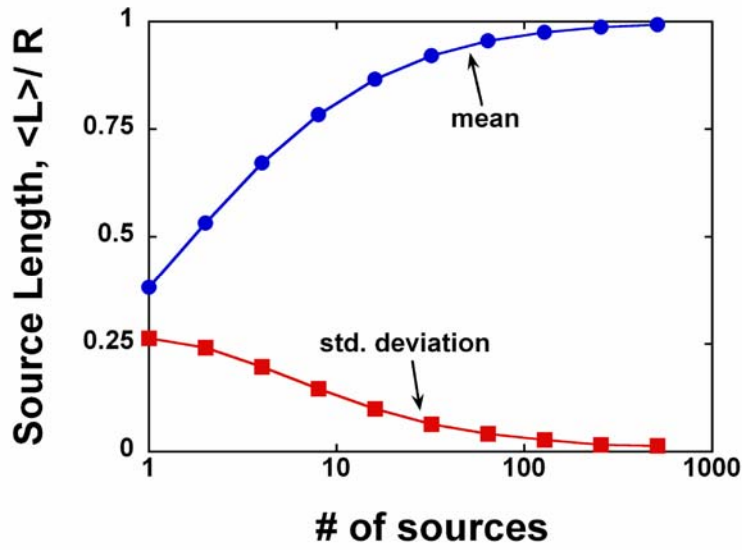
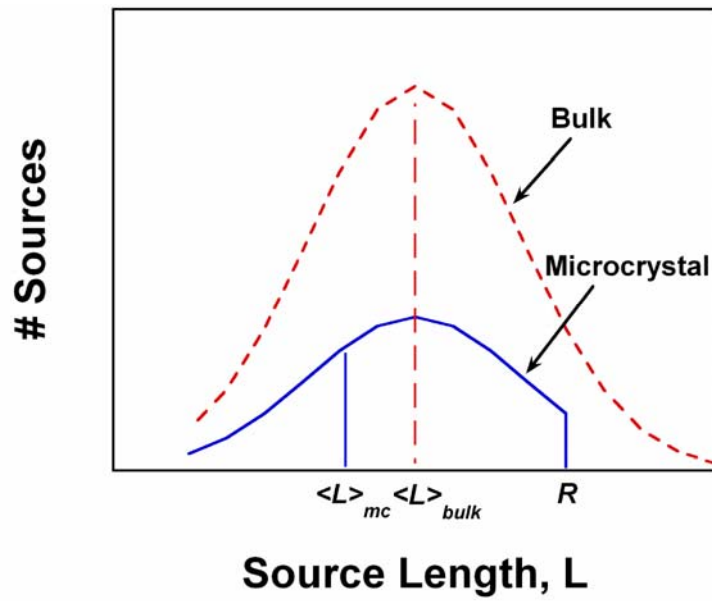


Figure 7: Critical resolved shear stress (τ^*) of 30° single-ended and double-ended (Frank-Read) sources as a function of length L of the sources. Also, shown are fits to the simulation data (solid lines), $\tau = k\mu \ln(L/b)/(L/b)$, where $k = 0.06$ (single ended backward); $k = 0.12$ (single ended forward) and $k = 0.18$ (double ended). All results are for the SSA method. Critical stresses are in MPa.



(a)



(b)

Figure 8: a) Average source length, $\langle L \rangle$, as well as the standard deviation in $\langle L \rangle$ (scaled to the radius of the sample, R) versus the number of initial mobile sources in the sample (based on an initial dislocation density, see [11]). b) Schematic illustration of source length distributions for microcrystals versus bulk samples following model given in [11].